Author/s:
Lu, J;Cheng, C;He, YS;Lyu, C;Wang, Y;Yu, J;Qiu, L;Zou, D;Li, D

Title:
Multilayered Graphene Hydrogel Membranes for Guided Bone Regeneration

Date:
2016-06-01

Citation:
Lu, J., Cheng, C., He, Y. S., Lyu, C., Wang, Y., Yu, J., Qiu, L., Zou, D. & Li, D. (2016). Multilayered Graphene Hydrogel Membranes for Guided Bone Regeneration. Advanced Materials, 28 (21), pp.4025-4031. https://doi.org/10.1002/adma.201505375.

Persistent Link:
https://hdl.handle.net/11343/291115

DOI: 10.1002/adma.201505375

Article type: Communication

Multilayered graphene hydrogel membranes for guided bone regeneration

Jiayu Lu, Chi Cheng, Yu–Shi He, Chengqi Lyu, Yufei Wang, Jia Yu, Ling Qiu, Derong Zou and Dan Li**

*To whom correspondence should be addressed.

J. Lu, C. Lyu, J. Yu, Prof. D. Zou
Department of Stomatology, Shanghai Jiao Tong University Affiliated Sixth People's Hospital, No. 600, Yishan Road, Xuhui District, Shanghai, 200233 (PR China)
E-mail: drzou@sjtu.edu.cn

Dr. C. Cheng, Dr. Y. Wang, Dr. L. Qiu, Prof. D. Li

Department of Materials Science and Engineering, Monash University, VIC 3800 (Australia)

E-mail: dan.li2@monash.edu

Dr. Y.-S. He
Shanghai Electrochemical Energy Devices Research Center, School of Chemistry and Chemical Engineering, Shanghai Jiao Tong University, Shanghai, 200240 (PR China)

Keywords: guided bone regeneration, osteoinductivity, osteoconductivity, graphene hydrogel membrane, multilayered architecture

Biomedical uses of emerging graphene-based bulk materials require collective consideration of various aspects of their properties and an understanding of how the materials architecture could favorably interact with components of the biological milieu. To date, few examples have successfully demonstrated clear advantages of engineering the architecture of graphene materials to deliver as many of their properties including extraordinary electrical, mechanical, thermal properties as intended for a targeted application (e.g. biomedical and regenerative engineering).[1] Here we show that a multilayer-nanostructured graphene hydrogel membrane can act as a barrier membrane for guided bone regeneration in a rat calvarial model. We found that the membrane can well adhere to the bone surface and maintain the space. The membrane was shown to promote early osteogenesis and accelerate mineralization for the regeneration of mature lamellar bone by the micro-CT and histological analyses at both an early observation time of 2 weeks and a final of 8 weeks after surgery. This encouraging osteoinductivity and osteoconductivity in vivo is attributed to both the osteogenic activity of chemically converted graphene and the unique multilayered architecture assembly, which offer a combination of advantageously balanced mechanical strength and flexibility, selective permeability and high bioactivity (beneficial to protein adsorption, cell adhesion and apatite deposition shown in in vitro study). These results not only confirm that chemically converted graphene is a promising material for bone regeneration, but also demonstrate that the architecture of graphene materials, if well engineered, can significantly enhance its performance in biomedical applications.

Graphene materials are seen as enabling components for medicine and biomedical devices not only because of their distinctive combination of many superior properties, such as mechanical strength, flexibility and controllable permeability, but also due to their versatile morphology (size, shape and chemistry) which offers numerous opportunities for complex and multifunctional application scenarios.[2,3] A number of studies demonstrated that the interaction and binding of various graphene material types onto stem cells can lead to a potential enhancement of cell attachment and growth, and differentiation into various lineages, such as osteoblasts, neurons, and myocytes.[4] However, it is the versatility of graphene materials that has made exploring the interface of graphene and biology challenging.[5] Research in understanding the behavior of graphene materials in biological systems for purposes ranging from imaging, biosensing, bioelectrode to tissue engineering has been traditionally focused on single sheets of graphene.[6] Yet, recent efforts on graphene assembly have led to graphene-based bulk materials that are endowed with both distinctive properties such as unprecedented mechanical strength and flexibility, porosity and oriented feature, and versatile macroscopic structures including 1D fibers, 2D membranes and 3D foams.[7-9] As these graphene bulk structures are comprised of a large number of graphene sheets assembled into a distinctive macroscopic structure, exploring these materials for biological uses also requires an understanding of the influence that the material architecture has on the biological response at multiple length scales of graphene-based bulk materials. Despite this, the question of how the architecture of graphene materials can be engineered to optimize the properties of graphene materials for in vivo biomedical applications, remains largely unexplored.[2,10]

Advanced biomedical treatment often has stringent requirements for the tools and materials

adopted. For example, in the biomedical practice of guided bone regeneration (GBR), an artificial barrier membrane is suggested to seal off the bone defect for a regeneration period of up to several weeks. Some kind of materials including titanium, polymer and other bioactive materials have been tried to fabricate the barrier membranes.[11] During the regeneration, the barrier membrane provides a sealed space to allow bone regeneration rather than the ingrowth of the surrounding fast-growing connective tissue.[12] The success of GBR, which is reflected by a higher regenerative potential than non-supported healing scenarios, depends on the properties of the barrier membrane materials to providing favorable interactions with osseous and surrounding tissues. The membrane materials are desired to have matching mechanical properties with bone tissues.[13] This means that the membrane needs to have balanced mechanical strength as being sufficiently strong helps maintain a secluded space for bone regeneration during the bone healing process, whilst, being flexible avoids damage to surrounding tissue and facilitates surgical operation.[11] The membrane is also expected to be selectively permeable to inflow of nutrients while preventing faster ingrowth of soft connective tissue cells.[14] In addition to being biocompatible, it is preferred that the membrane be actively osteogenic, favorably absorbs calcium phosphates and interfaces with proteins and cells so as to promote the differentiation of progenoitor cells to osteoblastic lineage (osteoinductive)[15] and provide a framework upon which to spread and generate new bone (osteoconductive).[16]

We have recently fabricated a graphene hydrogel (MGH) membrane comprised of multiple, face-to-face stacked chemically converted graphene (CCG) sheets (**Figure. 1**a,b).[17] This multilayered nano-architecture, to a certain extent, mimics the collagen fibers assembled with HA crystals in native cancellous and cortical bone.[18] The MGH membranes are strong yet flexible. The average

tensile modulus reaches 69 ± 5 MPa, which closes to the order of magnitude of that of rat braincase.[8, 19] Empirical evidence suggests that high mechanical strength has great potentials for osteoblast differentiation.[20] Moreover, because of the micro-corrugated texture of CCG, the MGH membranes can be made highly porous with a packing density as low as ~0.06 g/cm^3, which corresponds to an average interlayer spacing between CCG sheets of ~13 nm allowing liquids and small molecules to pass through.[17, 21, 22] Nano-channels of membrane materials have been proved to allow for the quick diffusion of glucose and other nutrients.[23] Due to the adaptive nature of hydrogel materials, it has been demonstrated that the MGH membranes shrink along thickness direction upon drying.[24] The multilayered microstructure of the MGH membranes collapses irreversibly to form a much denser structure when the water molecules trapped in between CCG layers are removed (Figure 1c). [24] This offers a simple avenue towards tuning the nano-architecture of such graphene membranes. In addition to the inherently osteogenic properties and biocompatibility that have been demonstrated for MGH,[8] it appears that the MGH membranes with advantageously mechanical and selective permeation properties as well as its easily definable material architecture could make it an attractive candidate for exploring the potential of graphene for GBR therapy. Therefore, in this study, we use MGH membranes, with defined graphene architecture, to investigate their performance in the specific biomedical module of guided bone regeneration.

We selected the widely used rat calvarial defect model as the standard to evaluate the bone regeneration performance of the MGH membranes.[13] In a typical rat calvarial defect model, a critical diameter of 5 mm circular defect was created (Figure 1d). A fracture of the defect of this size cannot be healed during the lifetime of the animal because rat calvaria lacks blood supply

and muscle tissue. In our experiment, we have tested three types of membrane materials in parallel, which included the MGH, collapsed MGH and titanium membranes for comparison. As titanium membranes have been adopted for clinical GBR therapy for more than twenty years, we used them as a standard by which the performance of our graphene materials was judged.[11] It is also worthwhile to point out that the MGH membranes and collapsed or dried MGH membranes share the same chemistry, lateral size distribution of individual sheets and the same mass loading of CCG. Compared to the MGH membranes with an average interlayer spacing between CCG sheets of ~13 nm, the collapsed MGH membranes have a much smaller average interlayer spacing of ~0.5 nm (see a schematic in Figure 1c). This gives us a unique advantage to investigate the sole effect of the pore structure of the architectured graphene materials on GBR outcome.

Once implanted, the MGH membranes were observed to be well adhered to the bone tissue surrounding the defect without the aid of additional grafting materials and fixation pins. Throughout the entire bone healing procedure, the MGH membranes remained in place and maintained their structural integrity in gross specimen examination. As the MGH membranes are hydrogels, they are more flexible and mechanically compatible with osseous and surrounding tissues than the rigid titanium membranes. This helps bring down the number of exposures caused by mucosal perforation. All the rats were found to remain in good health and did not show any wound complications throughout the eight weeks of experiment.

In order to study the quantity of the regenerated bone, the micro-CT scanning images and the analysis at the end of 8 weeks of implantation are shown in **figure 2**a,b. The results showed that a substantial amount of new bone is formed and is evenly distributed over the facture under the MGH membrane (Figure 2a). The bone volume fraction (BVF) of the MGH group was found to be significantly higher than that of all the other groups (Figure 2b). Furthermore, Van Gieson's staining of the undecalcified sections showed that nearly all the defect space in the MGH group was filled with confluent bone with a percentage of new bone area remarkably larger than the titanium membrane group and control group (Figure 2c and Figure S1). The MGH membrane provided a sealed space successfully to allow bone regeneration rather than the ingrowth of the surrounding fast-growing connective tissue.

Then, in order to understand the quality of the regenerated bone, bone mineral density (BMD) was analyzed as the major index to evaluate the quality and strength of regenerated bone. The BMD of the MGH membrane group reached 67.35% to that of normal rat calvaria (Figure 2b), significantly higher than all the other material groups tested. In addition, the trabecular thickness and trabecular separation analysis showed that the regenerated bone under the MGH membranes was noticeably uniform with the highest trabecular thickness of 0.30 ±0.06 mm and smallest trabecular separation of 0.22 ± 0.10 mm (Figure S2). Histological observation further verified the finding. Specifically, in the MGH group, a three-layered bone structure was readily visible and corresponded to a lamellar bone containing diploic bone surrounded by external and internal cortical bone with flattened lining osteoblasts (Figure 2c). In the diploic bone, small vascular structures and osteocytic lacunae containing osteocytes can be observed. This three-layered structure was very similar to that of the original bone tissue, which could also be

observed in the histomorphometric assessment. Fluorescent labeling evaluation (Figure 2d) showed that parallel linear fluorescences on both sides, to a certain extent, represented compact layers of the outer cortical bone, and circular fluorescences in the center represented osteons or trabeculars in the central diploic bone. These results suggested that mature and strong lamellar bone formed in the calvarial defect covered by the MGH membranes. But in other groups, no such mature bone tissue especially dense cortical bone was observed.

Calvarial defects in the untreated control group were bridged primarily by fibrous connective tissue and the bone formation was restricted to the edges of the host bone. Subtotal repair with immature bone is present in the titanium membrane group, and the remainder of the defect was spanned by fibrous connective tissue. In the collapsed MGH membrane group, the defects were closed almost entirely by immature lamellar bone. The new bone grown from the lateral margins contained a greater number of small vascular channels, which appeared to facilitate differentiation of the new bone from the host bone. No tissue resembling cartilage morphologically was observed in any group.

We also investigated the speed of bone regeneration using the fluorescent labeling technique. The yellow tetracycline labels were seen more pronounced in the MGH group than the others, which was a reflection of new bone formation after 2 weeks of operation (Figure 2d). This indicated that the MGH membranes showed appreciable osteogenesis at the earlier stage. The dynamic morphological observation by the fluorescent labeling analysis also showed that the value of mineral apposition rate (MAR) was significant higher in the MGH group both after 2-4

weeks (2.96 ± 0.86 μm/day) and 4-6 weeks (2.73 ± 0.81 μm/day) of surgery than that in titanium and control group (Figure 2e), and almost twice as fast as that in the titanium membrane group (1.59 ± 0.89 and 1.22 ± 0.37 μm/day respectively). On the other hand, we have noticed that in the collapsed MGH membrane group, the value of MAR was also statistically higher than that of the titanium membrane group and control group in the 4-6 weeks periods (Figure 2e). This suggests a reasonably fast mineralization speed of the collapsed MGH during the latter observation period and good bone regeneration which could also be testified by the newly formed bone grown into the center region (Figure 2a, c). In general, the graphene-based membranes have better ability of bone regeneration than the titanium membrane.

The rapid bone formation rate at an early stage was further confirmed by the micro-CT analysis after 2 weeks of implantation. The BVF of the 2 weeks samples in the MGH group was also found significantly higher than that in either the titanium membrane group or the control group (Figure S3). Meanwhile, the micro-CT image clearly shows that the new bone grew from the lateral margins and bone islands formed within the defects in both CCG membrane groups (both the MGH and collapsed MGH membranes, Figure S4). These results indicate that the membranes are indeed osteoconductive, guiding the bone formation from the lateral margins. At the early stage, the inherent osteoinductive membranes (Figure S5) stimulate stem cells in the center region to undergo osteogenic differentiation and induce bone formation, accelerating the new bone formation.

After 2 weeks of healing, the histological analysis shows no evidence of severe inflammatory responses in all the specimens (Figure S6). In the MGH membrane group, the newly formed bone generating from both the host bone and central nodules was obviously thicker and more abundant than that of other groups at an early stage. The residual bone defects were filled with fibrous connective tissue. The collagens in the MGH membrane group were more organized parallel to the membrane and appeared as thick collagen fibers forming a pretrabecular scaffold that dictated the direction of the new forming trabeculae, while the control defect was invaded by a loosely organized connective tissue (Figure S6).

We next seek insights into the effect of nano-architecture on bone formation. The early osteogenesis, the large quantity and high quality of the regenerated bone formed in the inherently osteoinductive CCG membrane groups (both the MGH and collapsed MGH membranes, Figure S4, S5) suggest that CCG is indeed a promising material for GBR therapy. The difference of the bone formation on the hydrated MGH membranes and collapsed ones indicates that the nano-architecture of the materials can also play a remarkable role in enhancing bone regeneration outcomes.

We conducted the protein adsorption and osteoblast adhesion experiments in vitro to shed light on the plausible mechanism how the nano-architecture of the MGH membrane affects the bone regeneration. As shown in **Figure 3**a and 3b, the protein adsorption and osteoblast adhesion of the MGH membranes are 2.5 and 2.8 times higher than those of the collapsed membranes. Apatite deposition in vitro, a key index known for evaluating the potential of in vivo osteogenic

bioactivity of a biomaterial,[25] was also found to be more pronounced on the MGH membranes: with the deposition on the MGH membrane readily observable 7 days after immersion in simulated body fluid (SBF). After 28 days of immersion, the crystalline apatite deposition layer has almost covered the whole surface of the membrane (Figure 3c and Figure S7), while on the collapsed MGH membranes and titanium membranes, no obvious apatite formed during the entire span of deposition test (Figure S8-S10).

Since the only difference between the MGH and collapsed membranes is that the MGH membranes have a larger average interlayer spacing (around tens of nanometers) than that of the collapsed ones (~0.5 nm), the improved performance of the MGH membrane can be attributed to the difference in nano-architecture. The collapsed MGH membranes have a much smaller interlayer spacing nearly impermeable to ions and biomolecules,[26] as such, it is suspected that the insufficient adsorption of the key nutrients that are crucial the formation of calcium phosphate that results in the lack of apaitate formation on the collapsed MGH membranes. On the other hand, the MGH membrane ensures complete cutoff of cell traffic but allows inflow of liquid and small nutrient molecules. In the practice of orthopedic applications such as GBR, early events like protein adsorption, cell adhesion and apatite formation are critical for subsequent osteoblast functions (from proliferation to differentiation and deposition of calcium-containing minerals).[27] Such bioactivity studies in vitro together with the osteogenesis performances in vivo verify the superior osteoconductivity of the MGH membranes over their collapsed counterparts. This result confirms that the multilayered nanoarchitecture, if properly engineered, can enhance the osteogenic bioactivity of CCG materials, and thus, bone regeneration performance.

In summary, we have used multilayered graphene membranes as a representative graphene material to explore their use for guided bone regeneration. The results suggest that CCG is a promising candidate material for GBR therapy. In particular, CCG based membranes can successfully maintain osseous space, promote early osteogenesis, and speed up mineralization and allow higher quality and fast bone regeneration (Figure 1e). Moreover, the selection of an appropriate multilayered nanostructure for the MGH membranes results in improved material properties, including mechanical strength, flexibility and selective permeability. The nanostructure enables the MGH membranes to interact with proteins resulting in improved osteoblast adhesion and apatite deposition. The MGH membranes were observed to remain in place after being implanted for 8 weeks, suggesting that the surface texture of MGH membranes could be favorable to their adhesion to bone tissues. This work effectively demonstrates the critical role and importance of engineering the architecture of graphene materials in order to extend the potential of this exciting class of materials for existing and emerging biomedical applications.

1. a) K. S. Novoselov , A. K. Geim , S. V. Morozov , D. Jiang , Y. Zhang , S. V. Dubonos , I. V. Grigorieva , A. A. Firsov , *Science* **2004** , *306* , 666 ; b) M. J. Allen , V. C. Tung , R. B. Kaner , *Chem. Rev*. **2010** , *110* , 132 ; c) A. A. Balandin , S. Ghosh , W. Z. Bao , I. Calizo , D. Teweldebrhan , F. Miao , C. N. Lau , *Nano Lett*. **2008** , *8* , 902 ; d) H. Shen , L. Zhang , M. Liu , Z. Zhang , *Theranostics* **2012** , *2* , 283 .

2. K. S. Novoselov , V. I. Fal'ko , L. Colombo , P. R. Gellert , M. G. Schwab , K. Kim , *Nature* **2012** , *490* , 192 .

3. a) A. K. Geim , *Science* **2009** , *324* , 1530 ; b) C. Chung , Y. K. Kim , D. Shin , S. R. Ryoo , B. H. Hong , D. H. Min , Acc. *Chem. Res*. **2013** , *46* , 2211 ; c) Y. Zhu , S. Murali , W. Cai , X. Li , J. W. Suk , J. R. Potts , R. S. Ruoff , *Adv. Mater*. **2010** , *22* , 3906 ; d) H. Xie , T. C , J. V. Gomes , A. H. C. Neto , V. Rosa , *Carbon* **2015** , *93* , 266; e) N. Dubey , R. Bentini , I. Islam , T. Cao , A. H. C. Neto , V. Rosa , *Stem Cells Int*. **2015** : 804213; f) H. Elkhenany , L. Amelse , A. Lafont , S. Bourdo , M. Caldwell , N. Neilsen , E. Dervishi , O. Derek , A. S. Biris , D. Anderson , M. Dhar , *J. Appl. Toxico*. doi:10.1002/jat.3024 ; g) E. Bressan , L. Ferroni , C. Gardin , L. S , L. Gobbato , F. S. Ludovichetti , I. Tocco , A. Carraro , A. Piattelli , B. Zavan , *J. Transl. Med*. **2014** , *12* , 296 .

4. T. H. Kim , T. Lee , W. A. El-Said , J. W. Choi , *Materials* **2015** , *8* , 8674 .

5. a) K. Kostarelos , K. S. Novoselov , *Science* **2014** , *344* , 261 ; b) C. Schmidt , *Nature* **2012** , *483* , S37 .

6. a) K. Yang , L. Feng , X. Shi , Z. Liu , *Chem. Soc. Rev*. **2013** , *42* , 530 ; b) X. Sun , Z. Liu , K. Welsher , J. T. Robinson , A. Goodwin , S. Zaric , H. Dai , *Nano Res.* **2008** , *1* , 203 ; c) Z. S. Siwy , M. Davenport , *Nature Nanotech*. **2010** , *5* , 697 ; d) T. R. Nayak , H. Andersen , V. S. Makam , C. Khaw , S. Bae ,X. Xu , P. R. Ee , J. Ahn , B. H. Hong , G. Pastorin , B. Özyilmaz , *ACS Nano* **2011** , *5* , 4670 ; e) W. Grosse , J. Champavert , S. Gambhir , G. G. Wallace , S. E. Moulton , *Carbon* **2013** , *61* , 467 .

7. Z. Xu , C. Gao , *Nat. Commun*. **2011** , *2* , 571 .

8. J. Lu , Y. He , C. Cheng , Y. Wang , L. Qiu , D. Li , D. Zou , *Adv. Funct. Mater*. **2013** , *23* , 3494 .

9. L. Qiu , J. Z. Liu , S.L.Y. Chang , Y. Wu , D. Li , *Nat. Commun*. **2012** , *3* , 1241 .

10. K. Kostarelos , K. S. Novoselov , *Nature Nanotech*. **2014** , *9* , 744 .

11. a) L. Molly , M. Quirynen , K. Michiels , D. Steenberghe , *Clin. Oral Impl. Res*. **2006** , *17* , 481 ; b) P. Gentile , V. Chiono , C. Tonda-Turo , A. M. Ferreira , G. Ciardelli , *Biotechnol. J*. **2011** , *6* , 1187 ; c) E. Tejeda-Montes , A. Klymov , M. R. Nejadnik , M. Alonso , J. C. Rodriguez-Cabello , X. F. Walboomers , *A. Mata , Biomaterials* **2014** , *35* , 8339 .

12. M. Retzepi , N. Donos , *Clin. Oral Impl. Res*. **2010** , *21* , 567 .

13. E. J. Lee , D. S. Shin , H. E. Kim , H. W. Kim , Y. H. Koh , J. H. Jang , *Biomaterials* **2009** , *30* , 743 .

14. A. L. Pinheiro , M. E. M. Gerbi , F. A. L. Jr , E. A. C. Ponzi , A. M. C. Marques , C. M. Carvalho , R. C. Santos , P. C. Oliveira , M. Nóia , L. M. P. Ramalho , *Lasers Med. Sci*. **2009** , *24* ,234 .

15. S. W. Choi , Y. Zhang , S. Thomopoulos , Y. Xia , *Langmuir* **2010** , *26* , 12126 .

16. M. Stevens , *Mater. Today* **2008** , *11* , 18 .

17. a) X. Yang , J. Zhu , L. Qiu , D. Li , *Adv. Mater*. **2011** , *23* , 2833 ; b) H. Chen , M. B. Müller , K. J. Gilmore , G. G. Wallace , D. Li , *Adv. Mater*. **2008** , *20* , 3557 .

18. a) L. Kong , Q. Ao , A. Wang , K. Gong , X. Wang , G. Lu , Y. Gong , N. Zhao , X. Zhang , *J. Biomater.Appl*. **2007** , *22* , 223 ; b) I. K. Yoon , J. Y. Hwang , J. Seo , W. C. Jang , H. W. Kim , U. S. Shin , *Carbon* **2014** , *77* , 379 .

19. C. E. Petrie Aronin , K. W. Sadik , A. L. Lay , D. B. Rion , S. S. Tholpady , R. C. Ogle , E. A. Botchwey , *J. Biomed. Mater. Res. Part A* **2009** , *89* , 632 .

20. A. J. Engler , S. Sen , H. L. Sweeney , D. E. Discher , *Cell* **2006** , *126* , 677 .

21. Y. Wang , S. Chen , L. Qiu , K. Wang , H. Wang , G. P . Simon , Dan Li , *Adv. Funct. Mater*. **2015** , *25* , 126 .

22. L. Qiu , X. Zhang , W. Yang , Y. Wang , G. P. Simon , Li. Dan , *Chem. Commun*. **2011** , *47* , 5810 .

23. K. M. Ainslie , T. A. Desai , *Lab Chip* **2008** , *8* , 1864 .

24.X. Yang , L. Qiu , C. Cheng , Y. Wu , Z. Ma , D. Li , *Angew. Chem. Int. Ed*. **2011** , *50* , 7325 .

25. T. Kokubo , H. Takadama , *Biomaterials* **2006** , *27* , 2907 .

26. Y. Su , V. G. Kravets , S. L. Wong , J. Waters , A. K. Geim , R. R. Nair , *Nat. Commun.* **2014** , *5* , 4843 .

27. a) P. A. Tran , L. Zhang , T. J. Webster , *Adv. Drug Deliv. Rev*. **2009** , *61* , 1097 ; b) R. W. Li , N. T. Kirkland , J. Truong , J. Wan , P. N. Smith , N, Birbilis , D. R. Nisbet , J. *Biomed. Mater. Res. Part A* **2014** , *102* , 4346 .

28. a) H. Chen , M. B. Müller , K. J. Gilmore , G. G. Wallace , D. Li , Adv. Mater. 2008 , 20 , 3557 ; b) D. Li , M. B. Müller , S. Gilje , R. B. Kaner , G. G. Wallace , *Nature Nanotechnology* **2008** , *3* , 101.

29. A. M. Parfitt , M. K. Drezner , F. H. Glorieux , J. A. Kanis , H. Malluche , P. J. Meunier , S. M. Ott , R. R. Recker , *J. Bone Miner. Res*. ***1987*** , *2* , 595 .

30. T. Kokubo , H. Takadama , *Biomaterials* **2006** , *27* , 2907 .

Experimental Section

Preparation of multilayered graphene hydrogel (MGH) membrane and collapsed MGH membrane. Chemically converted graphene (CCG) was synthesized by chemical reduction of a graphene oxide solution acquired by chemical oxidation and exfoliation of natural graphite using our previously reported method.[28] A certain amount of CCG dispersion (0.37 mg/mL) was then filtered through a mixed cellulose ester filter membrane (0.05 μm pore size; Millipore Co., USA) by vacuum filtration. Once the filtration was accomplished, the MGH membranes were carefully peeled off from the filter membrane using tweezers and stored in water prior to use. The membrane is highly porous and contains about 90% water. The pore size of the MGH membrane is ~13nm. The thickness of MGH membranes (with an areal mass loading of 1 mg/cm^2) is around 180 μm, tested using a digital micrometer caliper, and the average tensile

modulus of the membranes has previously been reported to be 69 ± 5 MPa, measured on a dynamic mechanical thermal analyzer (DMTA, Mark IV; Rheometrics, USA). To obtain the collapsed MGH membrane, the wet membranes were further vacuum-filtered until dry. Scanning electron microscopy (SEM) analysis of a freeze-dried sample revealed a uniform multilayered and wrinkled structure. All membranes were cut into required sizes using scissors and sterilized by autoclaving (125 °C/0.14 MPa, 30 min) prior to use. The titanium membrane used in the experiment is nonporous and the thickness of the membrane is 17 μm.

***In vivo* animal test.** *In vivo* test was performed on 24 male Fischer rats aged 8 weeks (body weight 270–300 g) using a previously described method. The experimental protocol was formally approved by the Animal Care and Experiment Committee of the Sixth Peoples Hospital affiliated to Shanghai Jiao Tong University, School of Medicine. All the animals were randomly divided into 5 groups: control group without any barrier membrane used (n=4); MGH membrane group (n=6); collapsed MGH membrane group (n=6); titanium membrane group (Zhongbang Biomaterial Inc., Xi'an, China) (n=6); unoperated group (n=2). Briefly, calvarial defects were generated using a trephine drill with a diameter of 5 mm on the bilateral sides of the midline in each animal. Both defects were covered with test membranes, which had been trimmed (a diameter of 7 mm) to completely cover the bone defects and extending onto the surrounding bone margins. Then the wounds were carefully sutured. In the control group, the defects were left without membranes.

Polyfluorochrome Sequential labeling. Polyfluorochrome sequential labeling was carried out to evaluate the speed of bone formation and mineralization. The rats received tetracycline hydrochloride (25 mg/kg) (Sigma, Chemical Co, St Lous, MO USA) subcutaneously 2 weeks postoperatively, and alizarin red s (30 mg/kg) (Sigma, Chemical Co, St Lous, MO USA) 4 weeks

postoperatively, respectively. By 2 weeks before sacrifice, calcein green (20 mg/kg) (Sigma, Chemical Co, St Lous, MO USA) was administrated subcutaneously.

Micro-CT scanning. To measure the condition of health of the animals, parameters included weighing and observation macroscopic signs of infection or other ailments during the healing period. Eight weeks after the calvarial defect operation, the rats were sacrificed and the defect sites were removed intact with the surrounding normal bone, prior to fixation in 10% neutral formaldehyde solution for 4 days. Each specimen was subjected to microcomputed tomography scanning using a desktop micro-CT device (eXplore Locus, GE HealthCare, USA). The micro-CT scanner was set at a voltage of 80 kV and a current of 80 μA. The micro-CT scanner's auxiliary software (Version ABA 2.2, GE Healthcare, USA) was used to make a three-dimensional (3D) reconstruction from sequential scans. A cylindrical region of a diameter of 5 mm and a height that covered the entire thickness of the calvarial bone was chosen as the region of interest (ROI). The bone volume fraction (BVF) was evaluated by the volume ratio of the mineralized tissue in ROI. Other micro-morphometric bone parameters were calculated including bone mineral density (BMD), trabecular thickness (Tb.Th: mm) and trabecular separation (Tb.Sp: mm) in ROI. In micro-CT scanning, the titanium membranes were displayed to cover the bone tissue from the superficial view of 3D images. Differing from the radiation resistance of titanium, carbonaceous materials are advantageous in radiotherapy as they are radiolucent and have minimal perturbation effects on the radiotherapy dose distribution. Consequently, the graphene membranes benefit from the assessment of bone formation with conventional radiographs, CT and MRI, which is important asset for monitoring the regeneration process non-invasively. In the titanium membrane group, we also found that, at the end of the investigated bone healing period, one specimen had lost its covering membrane. We suspect

that the loss resulted from the rigidity of titanium membranes, which leads to hard-hard interactions between the membranes and bone tissues. This can also be indirectly, but indicatively, reflected by the large standard deviation of the titanium group, which shows the relatively unstable osteogenic ability of the titanium membrane.

Histological observation. The specimens were dehydrated in ascending grades of ethanol and embedded in methylmethacrylate polymer (Sigma, Chemical Co, St Lous, MO USA). The specimens were cut and ground from the center of the defects perpendicular to the sagittal suture with Exact Cutting and Grinding Equipment (Exact Apparatebau, Norderstedt, Germany) to a thickness of 80 μm, based on the technique reported by Donath & Breuner. Fluorescent labeling was observed with the undecalcified sections under confocal laser scanning microscope (LSM710, CarlZeiss, Germany). To explore the bone formation and mineralization in the defects, fluorochrome staining of the newly formed bone was measured within the defect zone of 5mm in diameter. The images were stored digitally and then evaluated with an image analysis system (Image-Pro PlusTM 6.0, MD, USA). The parameter mineral apposition rate (MAR, μm/day) was quantified according to the American Society for Bone and Mineral Research histomorphometry nomenclature committee.[29]

After grinding to a thickness of 40μm, each section was further stained with Van Gieson's picric acid-fuchsin. The newly formed bone within the defect was quantitatively evaluated by using the Olympus light microscope (Olympus BX51, Tokyo, Japan) and analyzed with an image analysis system (Image-Pro PlusTM 6.0, MD, USA). Percentage of new bone area was calculated by determining the ratio of new bone area to total defect area.

Protein adsorption: The quantities of protein adsorbed onto the MGH, collapsed MGH and titanium membrane and glass tested in the present study were determined following immersion of each sample separately in Dulbecco's modified Eagle's medium (DMEM, Gibco, USA) supplemented with 50% fetal bovine serum (FBS, Gibco, USA) at 37 ^{o}C for 4 h. After the prescribed time period, each substrate gently was rinsed with phosphate buffered saline (PBS) at room temperature. Then adhering proteins were desorbed by soaking the substrate in 1% sodium dodecyl sulfate (SDS) for 15 min. The protein concentration in each eluant was subsequently determined using a commercially available kit (micro bicinchoninic acid (BCA) assay, Pierce). Experiments were run in triplicate.

Cells culture and cell adhesion: Osteoblasts were isolated via sequential collagenase digestions of neonatal rat calvaria, according to established protocols, and cultured in DMEM supplemented with 10% FBS. The experimental protocol was formally approved by the Animal Care and Experiment Committee of the Sixth Peoples Hospital affiliated to Shanghai Jiao Tong University, School of Medicine. The osteoblastic phenotype of these cells was determined by the alkaline phosphatase activity and the formation of calcium containing mineral deposits in the extracellular matrix. Osteoblasts at population numbers 3 were used in the experiment. The cells at a seeding density of 5×10^{3} cells/ membrane were resuspended in fresh culture medium, and then loaded on the substrates of interest for 4 h. At the end of the prescribed time period, nonadherent cells were removed by gently rinsing with PBS. Adherent cells were fixed in situ with 4% paraformaldehyde for 30 min. Then DAPI (2μg/mL) was mixed with each substrate for 10 min and then visualized under a fluorescence microscope (DMI6000B; Leica, Germany). Five random fields were selected and the number of DNA-intercalating fluorochrome DAPI was calculated.

Apatite-forming ability test on MGH membrane. After heating SBF to 36.5 °C, the MGH membranes and collapses membranes were submerged in the SBF according to established protocols.[30] After soaking at 36.5 °C for different periods within 4 weeks (1, 7 and 28days) in the SBF, the specimens were taken out, gently washed with pure water and examined by field emission scanning electron microscopy (SEM) (Nova NanoSEM 450, FEI, USA) equipped with energy dispersive X-ray spectroscopy (EDS, Apollo X, EDAX Inc.). All experiments were done in triplicate.

Statistical analysis. Statistically significant differences ($p < 0.05$) between the testing groups were measured by ANOVA and LSD post hoc or Kruskal-Wallis non-parametric procedure followed by Mann-Whitney U test for multiple comparisons according to the normal distribution and equal variance assumption test. All statistical analysis of data was carried out by SPSS (SPSS 19.0, Chicago, IL, USA) statistical software packages. All the data are shown as mean values ± standard deviation.

Supporting Information

Supporting Information is available from the Wiley Online Library or from the author.

Acknowledgements

The authors acknowledge the financial support from the Australian Research Council, the Science and Technology Commission of Shanghai Municipality (12JC1407301, 15410722600), Shanghai Natural Science Foundation (12ZR1447200), Doctorial innovation fund of medicine school of Shanghai Jiaotong University and the Natural Science Foundation of China (31400825, 81470714, 21336003, 21006063). We thank Xiu-Li Zhang for the help with specimens cutting.

Author information

These authors contributed equally to this work

Jiayu Lu & Chi Cheng & Yu-Shi He

Received: ((will be filled in by the editorial staff))
Revised: ((will be filled in by the editorial staff))
Published online: ((will be filled in by the editorial staff))

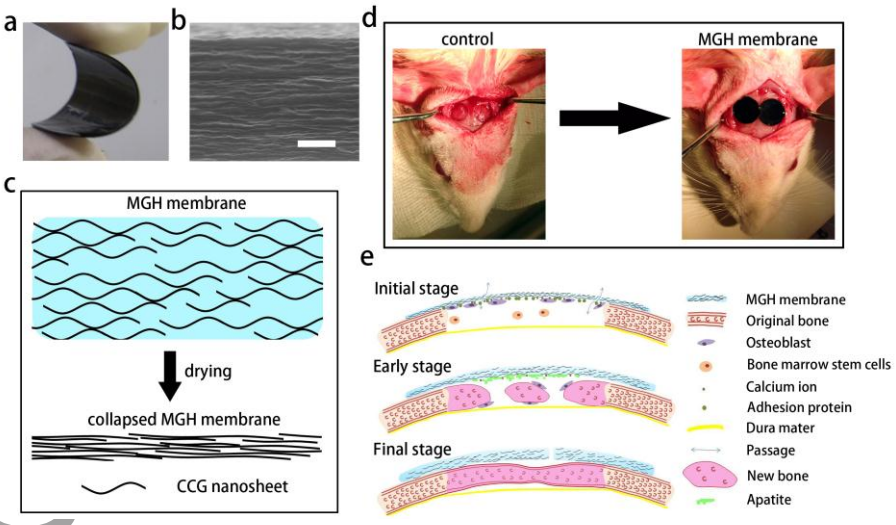

Figure 1. The structure of the CCG based membranes and schematics of the MGH membranes on GBR model of calvarial defect of rat. a) Photograph of the flexible MGH membrane; b) SEM image of the cross-section of a freeze-dried MGH membrane; Scale bar, 1 μm. c) Schematic of the cross-section of the MGH membrane showing that water molecules are trapped in between CCG

layers. After drying, the multilayered nano-architecture of MGH membrane collapses to form a highly densified structure. d) Schematic of the surgical operation that places the MGH membranes to seal off the calvarial defects of rat; e) Proposed GBR healing process of a calvarial defect using the MGH membranes as a barrier membrane. At the initial stage after bone trauma (from immediate to 1 day), the MGH membrane absorbs calcium ions, proteins and osteoblasts, promoting the activity of bone formation cells, the deposition of bone matrix and early bone formation. From 1 to 4 weeks (early stage), the membrane accelerates mineralization and the formation of apatite. The new bone formation appeared in both the lateral margin and the center region. At the final stage (after 8 weeks of operation), the newly formed bone with mature lamellar bone structure can be found across almost all the defect areas.

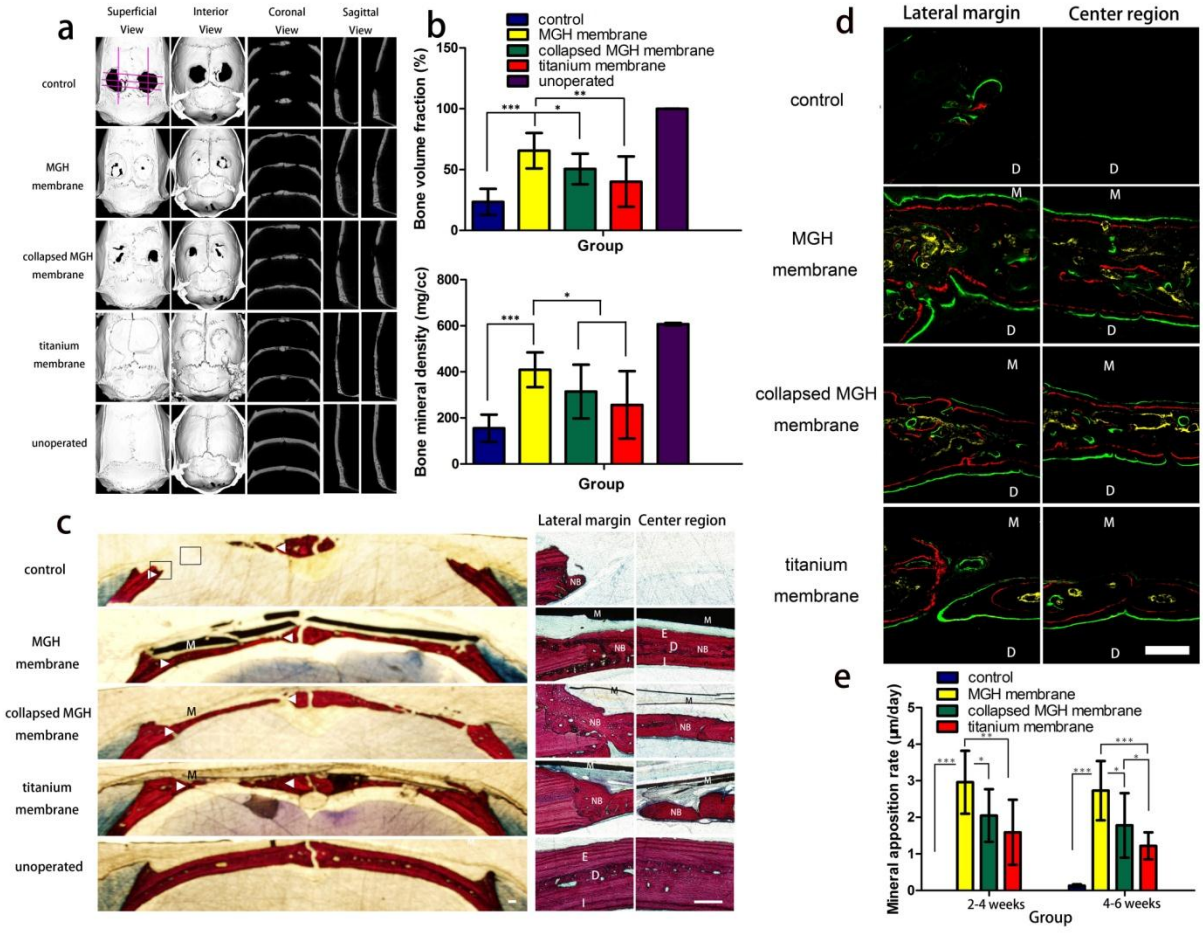

Figure 2. The bone regeneration 8 weeks after surgery. a) Micro-morphometric analysis of treated calvarial defects including superficial, interior, coronal and sagittal section views of micro-CT images taken at the 8th week after surgery. b) Micro-morphometric bone parameters including bone volume fraction and bone mineral density analyzed after eight weeks of surgery. Note that both the bone volume fraction and mineral density of the MGH membranes group are higher than the rest of the groups analyzed. c) Van Gieson's staining of calvarial undecalcified sections after 8 weeks of implantation. Low-magnification histological images (left) showed osteogenesis of the testing groups with/without barrier membranes (M). High magnification histology (right) showed boxed areas in the left images both the lateral margin and center

region of defects. In the MGH membrane group, the newly formed bone (NB) exhibited a mature lamellar bone structure with external cortical bone (E), diploic bone (D), and internal cortical bone (I) all discernable. Triangles denote the original bone margins. Scale bars, 250 μm. d) Fluorochrome labeling histomorphometric change analysis showed three-colored fluorescence in the lateral margin and center region of the defects rendering the newly formed bone in between the membrane side (M) and dura side (D). The yellow tetracycline labels were given earliest after 2 weeks of surgery, then alizarin red and green calcein labels were given after 4 weeks and 6 weeks of surgery, respectively. e) Mineral apposition rate, after 2 to 4 weeks and 4 to 6 weeks of surgery, respectively. Scale bar, 200 μm. Mean values ± standard deviation. (*P < 0.05; **P < 0.01 ; ***P < 0.001) determined by non-parametric procedure.

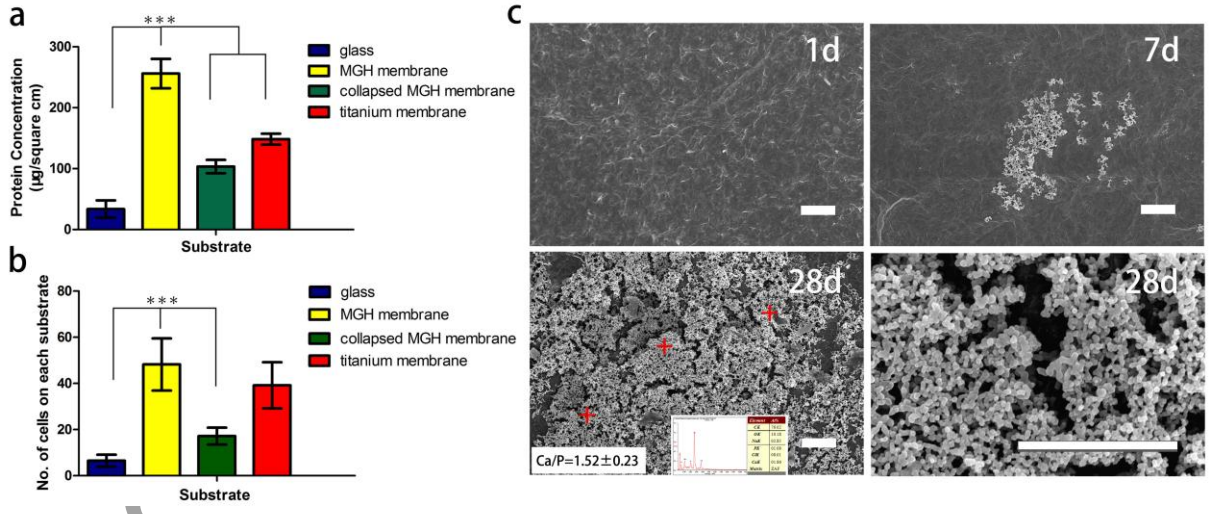

Figure 3. Bioactivities with protein adsorption, cell adhesion and apatite formation of the testing membranes. a) Protein adsorption of different substrates, measured after 4 h immersion in Dulbecco's modified Eagle's medium (DMEM) with 50% FBS. b) Osteoblasts adhesion on the

substrates 4 h after seeding. c) SEM images and energy dispersive X-ray spectrum (EDX) of apatite formed on the MGH membranes in simulated body fluid (SBF) for 1 day, 7 days and 28 days. Ca/P ratio of spots (+, n=3) on the membranes after immersion in SBF was reported. Scale bars, 2 μm. Mean values ± standard deviation. (***P < 0.001) measured by one-way ANOVA.

A multilayered graphene hydrogel membrane (MGH) has been used as an excellent barrier membrane for guided bone regeneration. The appropriate multilayered nanostructure of the MGH membrane results in improved material properties, which benefits to protein adsorption, cell adhesion and apatite deposition, and allows higher quality and fast bone regeneration.